

Constraining inflation with nonminimal derivative coupling with the Parkes Pulsar Timing Array third data release

Chang Han^{1,2}, Li-Yang Chen^{3,1,2}, Zu-Cheng Chen^{1,2,*}, Chengjie Fu^{4,†}, Puxun Wu^{1,2,‡}, Hongwei Yu^{1,2,§},
N. D. Ramesh Bhat⁵, Xiaojin Liu⁶, Valentina Di Marco^{7,8,9}, Saurav Mishra¹⁰, Daniel J. Reardon^{10,11},
Christopher J. Russell¹², Ryan M. Shannon^{10,11}, Lei Zhang^{13,10}, Xingjiang Zhu^{6,14} and Andrew Zic^{9,11}

(The PPTA Collaboration)

¹*Department of Physics and Synergetic Innovation Center for Quantum Effects and Applications, Hunan Normal University, Changsha, Hunan 410081, China*

²*Institute of Interdisciplinary Studies, Hunan Normal University, Changsha, Hunan 410081, China*

³*College of Physics and Engineering Technology, Chengdu Normal University, Chengdu, Sichuan 611130, China*

⁴*Department of Physics, Anhui Normal University, Wuhu, Anhui 241002, China*

⁵*International Centre for Radio Astronomy Research, Curtin University, Bentley, WA 6102, Australia*

⁶*Department of Physics, Faculty of Arts and Sciences, Beijing Normal University, Zhuhai 519087, China*

⁷*School of Physics and Astronomy, Monash University, Clayton VIC 3800, Australia*

⁸*OzGrav: The ARC Center of Excellence for Gravitational Wave Discovery, Clayton VIC 3800, Australia*

⁹*Australia Telescope National Facility, CSIRO, Space and Astronomy, PO Box 76, Epping, NSW 1710, Australia*

¹⁰*Centre for Astrophysics and Supercomputing, Swinburne University of Technology, P.O. Box 218, Hawthorn, VIC 3122, Australia*

¹¹*OzGrav: The ARC Centre of Excellence for Gravitational Wave Discovery, Hawthorn VIC 3122, Australia*

¹²*CSIRO Scientific Computing, Australian Technology Park, Locked Bag 9013, Alexandria, NSW 1435, Australia*

¹³*National Astronomical Observatories, Chinese Academy of Sciences, A20 Datun Road, Chaoyang District, Beijing 100101, China*

¹⁴*Institute for Frontier in Astronomy and Astrophysics, Beijing Normal University, Beijing 102206, China*

We study an inflation model with nonminimal derivative coupling that features a coupling between the derivative of the inflaton field and the Einstein tensor. This model naturally amplifies curvature perturbations at small scales via gravitationally enhanced friction, a mechanism critical for the formation of primordial black holes and the associated production of potentially detectable scalar-induced gravitational waves. We derive analytical expressions for the primordial power spectrum, enabling efficient exploration of the model parameter space without requiring computationally intensive numerical solutions of the Mukhanov-Sasaki equation. Using the third data release of the Parkes Pulsar Timing Array (PPTA DR3), we constrain the model parameters characterizing the coupling function: $\phi_c = 3.7^{+0.3}_{-0.5} M_{\text{P}}$, $\log_{10} \omega_L = 7.1^{+0.6}_{-0.3}$, and $\log_{10} \sigma = -8.3^{+0.3}_{-0.6}$ at 90% confidence level. Our results demonstrate the growing capability of pulsar timing arrays to probe early Universe physics, complementing traditional cosmic microwave background observations by providing unique constraints on inflationary dynamics at small scales.

I. INTRODUCTION

The inflationary paradigm has become a cornerstone of modern cosmology, providing elegant solutions to several fundamental puzzles, including the horizon, flatness, and monopole problems, in the early Universe [1–4]. While the standard slow-roll (SR) inflation successfully explains the observed cosmic microwave background (CMB) anisotropies [5, 6], there is growing interest in inflation models that can produce enhanced curvature perturbations at small scales. Such enhancement is particularly crucial for the formation of primordial black holes

(PBHs) [7–9], which have emerged as compelling candidates for dark matter and potential sources of gravitational wave (GW) events detected by LIGO-Virgo-KAGRA Collaboration [10–12]. The possibility of simultaneously explaining dark matter through PBHs and generating observable GW signatures provides a powerful probe of early Universe physics [13, 14].

Pulsar Timing Arrays (PTAs) have opened a new frontier in testing early Universe scenarios. In 2023, major PTA collaborations, including the European PTA (EPTA) in combination with Indian PTA (InPTA) [15, 16], the North American Nanohertz Observatory for GWs (NANOGrav) [17, 18], the Parkes PTA (PPTA) [19, 20], and the Chinese PTA (CPTA) [21], independently reported evidence for a stochastic GW background (SGWB) with Hellings-Downs spatial correlations [22]. Most recently, the MeerKAT PTA (MPTA) has also reported similar results [23, 24]. These observations re-

* zuchengchen@hunnu.edu.cn

† fucj@ahnu.edu.cn

‡ pxwu@hunnu.edu.cn

§ hwyu@hunnu.edu.cn

veal a common-spectrum process with a characteristic strain amplitude of approximately $\mathcal{O}(10^{-15})$ at a reference frequency of 1 yr^{-1} . While this signal is commonly attributed to GWs from supermassive black hole binaries (SMBHBs) [25–27], it may alternatively arise from primordial sources [28–32], offering a complementary window into inflationary dynamics.

Large-amplitude curvature perturbations at small scales not only result in PBHs formation but also generate significant scalar-induced GWs (SIGWs) [33–35], which have been extensively studied as potential explanations for the PTA signal [36–51]. Various inflationary models for amplifying small-scale curvature perturbations have been proposed, based on mechanisms such as ultra-slow-roll (USR) inflation [52–54], reduced sound speed [55, 56], and parametric resonance [57–59]. Among these, a novel model [60, 61] achieves USR inflation through the mechanism of gravitationally enhanced friction, which originates from a field derivative coupling with the Einstein tensor (known as nonminimal derivative coupling) [62–64]. A notable feature of this model is that the enhanced curvature perturbations exhibit an approximately broken power-law spectrum, with spectral indices that can be expressed analytically in terms of the model parameters [61]. This analytical tractability is particularly valuable, as linking specific models to observational data is often hindered by computational challenges that limit systematic parameter space exploration.

In this work, we use the PPTA third data release (DR3) to constrain the inflationary model with nonminimal derivative coupling proposed in [60]. We derive an analytical expression for the primordial power spectrum to facilitate efficient parameter estimation. The paper is organized as follows. In Sec. II, we develop the theoretical framework, presenting both analytical expressions for the primordial power spectrum and detailed calculations of the resulting SIGW energy density spectrum. Sec. III describes our methodology for analyzing the PPTA DR3 data. Sec. IV presents our results and discusses their implications for early Universe physics. Technical details are provided in Appendices A, B and C.

II. INFLATION WITH NONMINIMAL DERIVATIVE COUPLING

In this section, we investigate the model of inflation with nonminimal derivative coupling capable of generating enhanced primordial curvature perturbations, which subsequently lead to observable SIGWs. We begin by establishing the theoretical framework and analyzing the background evolution equations. We then derive analytical expressions for the primordial power spectrum and calculate the resulting GW energy density spectrum.

The action for the inflation model with nonminimal

derivative coupling is given by [60]

$$S = \int d^4x \sqrt{-g} \left[\frac{1}{2\kappa^2} R - \frac{1}{2} (g^{\mu\nu} - \kappa^2 \theta G^{\mu\nu}) \partial_\mu \phi \partial_\nu \phi - V(\phi) \right], \quad (1)$$

where $\kappa^{-1} \equiv M_{\text{P}} = 2.4 \times 10^{18}$ GeV is the reduced Planck mass. The ϕ is the scalar field value and the coupling function θ is chosen to provide localized enhanced friction between the inflaton field and gravity, and takes the form

$$\theta = \frac{\omega}{\sqrt{\kappa^2 \left(\frac{\phi - \phi_c}{\sigma} \right)^2 + 1}}. \quad (2)$$

Here, ω is a dimensionless parameter determining the maximum amplitude of the coupling, σ is a dimensionless parameter controlling the width of the coupling region, and ϕ_c is a mass scale parameter specifying the field value where the coupling reaches its maximum strength.

In the spatially flat Friedmann-Robertson-Walker (FRW) spacetime, the background evolution is governed by

$$3H^2 = \kappa^2 \left[\frac{1}{2} (1 + 9\kappa^2 H^2 \theta) \dot{\phi}^2 + V \right], \quad (3)$$

$$(1 + 3\kappa^2 H^2 \theta) \ddot{\phi} + 3H \left[1 + \kappa^2 (3H^2 + 2\dot{H}) \theta \right] \dot{\phi} + \frac{3}{2} \kappa^2 \theta_{,\phi} H^2 \dot{\phi}^2 + V_{,\phi} = 0, \quad (4)$$

where $H \equiv \dot{a}/a$ is Hubble parameter, and $a = e^N$ is the scale factor with $N = \int H(t) dt$ being the e-folding number. The specific form of coupling function θ given in Eq. (2) is crucial in generating a region of enhanced gravitational friction near $\phi = \phi_c$. Within this region, the inflaton field experiences substantially stronger friction compared to conventional SR regions, naturally transitioning into an USR stage of inflation. This mechanism produces a significant enhancement in the curvature perturbation power spectrum during the USR stage. As illustrated in Fig. 2, the resulting power spectrum exhibits three distinct stages: an initial SR stage with standard amplitude, a transition period, and an USR stage characterized by substantial enhancement.

A. Primordial power spectrum

We employ a fractional power-law potential

$$V = \lambda M_{\text{P}}^{4-p} |\phi|^p \quad (5)$$

with $p = 2/5$ [65], which ensures compatibility with current CMB constraints on the scalar spectral index at large scales [60, 61]. Under the SR and USR approximation, the curvature perturbation power spectrum takes

the analytical form [60]

$$\mathcal{P}_{\mathcal{R}}(\phi) \simeq \frac{\lambda}{12\pi^2 p^2} \left(\frac{\phi}{M_{\text{P}}} \right)^{2+p} \times \left[1 + \frac{\omega\lambda}{\sqrt{\kappa^2 \left(\frac{\phi - \phi_c}{\sigma} \right)^2 + 1}} \left(\frac{\phi}{M_{\text{P}}} \right)^p \right]. \quad (6)$$

This power spectrum can be approximated by a broken power-law form:

$$\mathcal{P}_{\mathcal{R}}(k) \simeq \begin{cases} k^{n_1}, & (k < k_p) \\ k^{n_2}, & (k > k_p) \end{cases} \quad (7)$$

with the spectral indices given by

$$n_1 = 3 \left(1 - \sqrt{1 - \frac{4}{15} (\kappa\phi_c)^{-7/5} (\omega\lambda\sigma)^{-1}} \right), \quad (8)$$

$$n_2 = 3 \left(1 - \sqrt{1 + \frac{4}{15} (\kappa\phi_c)^{-7/5} (\omega\lambda\sigma)^{-1}} \right).$$

The broken power-law approximation matches well with the results obtained by numerically solving Mukhanov-Sasaki equation [61].

The calculation of the SIGW energy spectrum using Eq. (19) in the following requires an explicit expression for the curvature power spectrum $\mathcal{P}_{\mathcal{R}}$ as a function of wavenumber k . This necessitates establishing a mapping between the inflaton field value ϕ and k . Traditionally, this mapping has been obtained by numerically solving the Mukhanov-Sasaki equation [66]:

$$u_k'' + (c_s^2 k^2 - \frac{z''}{z}) u_k = 0, \quad (9)$$

where c_s is sound speed and $u_k \equiv z\mathcal{R}_k$ (see Appendix A for a detailed derivation). While this numerical approach provides accurate results, it is computationally intensive, typically requiring several minutes of computation time for each set of model parameters. This computational overhead makes systematic exploration of the parameter space impractical. To address this limitation, we develop an analytical approximation for the ϕ - k mapping below.

First, let us discuss the relationship between the inflaton field ϕ and the e-folding number N . By combining the results obtained in [61], one can derive an approximate solution for Eqs. (3) and (4) (see Appendix B for details), expressed as:

$$\frac{H}{\dot{\phi}} \simeq \begin{cases} -\frac{\kappa^2 V (1 + \kappa^4 V \theta)}{V_{,\phi}}, & \text{for SR stage,} \\ -\frac{\kappa^2 V (3(1 + \kappa^4 V \theta) + \sqrt{6\theta_{,\phi} V_{,\phi} + 9(1 + \kappa^4 V \theta)^2})}{6V_{,\phi}}, & \text{for Transition stage,} \\ -\frac{\kappa^6 V^2 \theta}{V_{,\phi}}, & \text{for USR stage.} \end{cases} \quad (10)$$

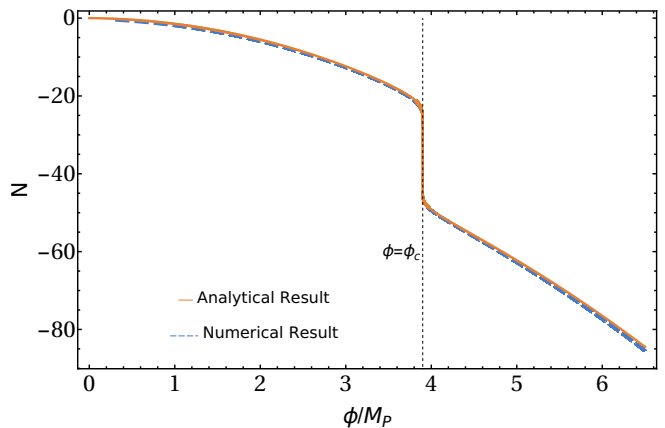


FIG. 1. Relationship between the e-folding number N and the inflaton field value ϕ for parameters $\phi_c/M_{\text{P}} = 3.9$, $\omega\lambda = 1.53 \times 10^7$, and $\sigma = 3 \times 10^{-9}$. The orange line shows our analytical solution $N(\phi)$, while the blue line represents the numerical result from solving the Mukhanov-Sasaki equations. The vertical dashed line indicates $\phi = \phi_c$.

Since the e-folding number N follows the relation,

$$N = \int_{t_{\text{end}}}^t H(\tilde{t}) d\tilde{t} = \int_{\phi_{\text{end}}}^{\phi} \frac{H}{\dot{\phi}}(\tilde{\phi}) d\tilde{\phi}, \quad (11)$$

where ϕ_{end} can be neglected for large-field inflation, a mapping from ϕ to N can be derived. After performing the necessary approximations and integration, one can obtain the function of $N(\phi)$ (see Appendix C for details). Fig. 1 demonstrates the excellent agreement between our analytical approximation and numerical results.

Using the horizon-crossing condition $c_s k = aH$ (where $c_s \simeq 1$), we can establish the relationship between the comoving wavenumber k and the field value ϕ through

$$k(\phi) = H(\phi) a(\phi) = H(\phi) \exp \left[\int_{\phi_{\text{end}}}^{\phi} \frac{H}{\dot{\phi}}(\tilde{\phi}) d\tilde{\phi} \right]. \quad (12)$$

The complete expressions and detailed derivation are provided in Appendices B and C. By inverting this relation to obtain $\phi(k)$ [given explicitly by Eq. (C11)] and substituting into Eq. (6), we obtain the power spectrum as a function of k . Fig. 2 demonstrates that this analytical result (orange line) closely matches the numerical solution of the Mukhanov-Sasaki equation (blue line) for representative parameters $\phi_c = 3.9 M_{\text{P}}$, $\omega\lambda = 1.53 \times 10^7$, and $\sigma = 3 \times 10^{-9}$, which proves that our expression is valid and can replace the numerical solution process. Furthermore, the derived spectral indices are consistent with those reported in [61].

B. Scalar-induced gravitational wave

SIGWs are generated by second-order effects when primordial curvature perturbations reenter the horizon dur-

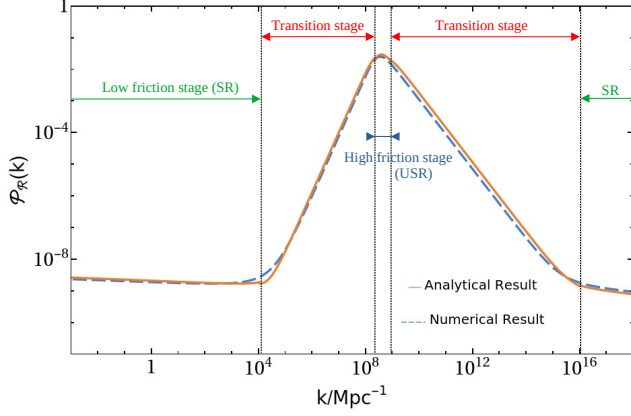


FIG. 2. Primordial power spectrum $\mathcal{P}_{\mathcal{R}}(k)$ for the same parameter values as in Fig. 1. The orange line shows our analytical result, while the blue line represents the numerical solution of the Mukhanov-Sasaki equations.

ing the radiation-dominated era. We consider perturbations to a FRW metric in the conformal Newtonian gauge [33]:

$$ds^2 = a^2 \left\{ -(1 + 2\Psi)d\tau^2 + \left[(1 - 2\Psi)\delta_{ij} + \frac{1}{2}h_{ij} \right] dx^i dx^j \right\}, \quad (13)$$

where τ is conformal time, Ψ denotes the Bardeen potential characterizing scalar perturbations, and h_{ij} represents tensor perturbations.

After reheating, the tensor perturbations are governed by the Einstein equations, with the spatial components yielding

$$h''_{ij} + 2\mathcal{H}h'_{ij} - \nabla^2 h_{ij} = -4T_{ij}^{lm} S_{lm}, \quad (14)$$

where primes denote derivatives with respect to τ , $\mathcal{H} \equiv a'/a$ is the conformal Hubble parameter, and T_{ij}^{lm} is the transverse-traceless projection operator [33]. The source term S_{ij} is given by

$$S_{ij} = 4\Psi\partial_i\partial_j\Psi + 2\partial_i\Psi\partial_j\Psi - \frac{1}{\mathcal{H}^2}\partial_i(\mathcal{H}\Psi + \Psi')\partial_j(\mathcal{H}\Psi + \Psi'). \quad (15)$$

For a given comoving wave number k , the scalar perturbation $\Psi(\tau)$ satisfies

$$\Psi''_k + \frac{4}{\tau}\Psi'_k + \frac{k^2}{3}\Psi_k = 0. \quad (16)$$

An analytical solution is

$$\Psi_k(\tau) = \psi_k \frac{9}{(k\tau)^2} \left(\frac{\sin \frac{k\tau}{\sqrt{3}}}{\sqrt{3}} - \cos \frac{k\tau}{\sqrt{3}} \right), \quad (17)$$

where ψ_k is the primordial perturbation. Therefore the power spectrum of curvature perturbations could be expressed as

$$\langle \psi_k \psi_{\tilde{k}} \rangle = \frac{2\pi^2}{k^3} \frac{4}{9} \mathcal{P}_{\mathcal{R}}(k) \delta(k + \tilde{k}). \quad (18)$$

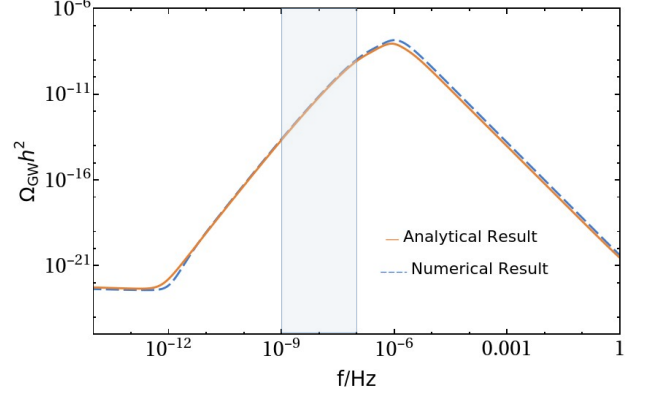


FIG. 3. Present-day energy density spectrum of SIGWs, $\Omega_{\text{GW}}h^2$, as a function of frequency. Results are shown for model parameters $\phi_c = 3.9 M_{\text{P}}$, $\omega\lambda = 1.53 \times 10^7$, and $\sigma = 3 \times 10^{-9}$. The orange line represents calculations using our analytical expression for $\mathcal{P}_{\mathcal{R}}(k)$, while the blue line shows the full numerical solution. The light blue shaded region indicates the frequency range accessible to PTA observations ($\sim 10^{-9}$ – 10^{-7} Hz).

The energy density of the SIGW could be related with power spectrum as [35]

$$\Omega_{\text{GW}}(\tau_c, k) = \frac{1}{12} \int_0^\infty d\nu \int_{|1-\nu|}^{1+\nu} du \left(\frac{4\nu^2 - (1 + \nu^2 - u^2)^2}{4\nu u} \right)^2 \times \mathcal{P}_{\mathcal{R}}(uk) \mathcal{P}_{\mathcal{R}}(\nu k) \left(\frac{3}{4u^3\nu^3} \right)^2 (-3 + u^2 + \nu^2)^2 + \pi^2 (-3 + u^2 + \nu^2)^2 \Theta(v + u - \sqrt{3}), \quad (19)$$

where Θ is the Heaviside theta function, and τ_c is the time of the SIGW stop grow. As the GW propagates to the present time, the energy density decreases as [67]

$$\Omega_{\text{GW}}h^2 = 0.83 \left(\frac{g_c}{10.75} \right)^{-\frac{1}{3}} \Omega_{r,0}h^2 \Omega_{\text{GW}}(\tau_c, k), \quad (20)$$

where $g_c \simeq 106.75$ represents the effective relativistic degrees of freedom at τ_c , and $\Omega_{r,0}h^2 \simeq 4.2 \times 10^{-5}$ is the present radiation density parameter. The frequency-wavenumber relation is given by

$$f = 1.546 \times 10^{-15} k \frac{\text{Hz}}{\text{Mpc}^{-1}}. \quad (21)$$

The energy density of SIGWs, Ω_{GW} , exhibits a quadratic dependence on the primordial power spectrum $\mathcal{P}_{\mathcal{R}}$. Consequently, the enhancement of scalar perturbations through nonminimal derivative coupling leads to a significant amplification of the SIGW signal. As shown in Fig. 3, we compare the SIGW energy density spectrum calculated using Eq. (20) for both our analytical solution of $\mathcal{P}_{\mathcal{R}}(k)$ (orange line) and the full nu-

merical computation (blue line). The excellent agreement between these results within the PTA-sensitive frequency range ($\sim 10^{-9}$ – 10^{-7} Hz) validates our analytical approach for predicting observable SIGW signals. In the PTA-sensitive frequency range, the relative error of $\Omega_{\text{GW}}h^2$ between analytical and numerical results remains at $\lesssim \mathcal{O}(10\%)$, and notably decreases with increasing ϕ_c . This analytical formulation represents a significant improvement over previous work [68], where relative errors could exceed an order of magnitude. Moreover, the relative error in the power-law index $n_s \equiv d \ln \Omega_{\text{GW}} / d \ln f$ remains at $\lesssim \mathcal{O}(1\%)$ across all model parameter choices in the PTA-sensitive range.

Our nonminimal derivative coupling model is characterized by three parameters: ϕ_c , $\omega_L \equiv \omega\lambda$, and σ . The physical consistency of the model imposes the constraint $\frac{4}{15}(\kappa\phi_c/M_{\text{P}})^{-1-p}(\sigma\omega_L)^{-1} < 1$, which avoids imaginary solutions and significantly restricts the available parameter space. Additional theoretical and observational constraints require $\frac{12}{25}(\kappa\phi_c/M_{\text{P}})^{-1-p}(\sigma\omega_L)^{-1} > 1$ and $3 < \phi_c/M_{\text{P}} < 4$, ensuring consistency with CMB observations while maintaining SIGW amplitudes within PTA-detectable ranges. The normalization parameter λ is conventionally determined by the CMB-scale power spectrum at $k^* \simeq 0.05 \text{ Mpc}^{-1}$, where observations indicate $\mathcal{P}_{\mathcal{R}}(k^*) \simeq 2.10 \times 10^{-9}$. In the standard SR inflation without coupling, $\lambda \approx 3.76 \times 10^{-10}$. However, the presence of nonminimal derivative coupling induces a slight enhancement of the spectrum at CMB scales and affects the evolution of the scalar field, necessitating a modification of λ . We adopt $\lambda = 8.0 \times 10^{-10}$ to accommodate this enhancement while maintaining consistency with observations.

III. DATA ANALYSIS

We use the PPTA DR3 [19] to constrain parameters of our nonminimal derivative coupling inflation model. PPTA DR3 encompasses 18 yr of high-precision timing observations from 2004 to 2022. The dataset includes 32 millisecond pulsars, of which 30 are used in this analysis after excluding PSR J1824–2452A (due to strong intrinsic red noise) and PSR J1741+1351 (insufficient observations) following [20]. The observations were conducted using the Parkes 64-meter radio telescope (now known as ‘Murriyang’), with recent significant enhancement through the ultrawide-band low (UWL) receiver system. This new instrumentation provides improved timing precision through wider bandwidth observations (704 ~ 4032 MHz). The data release extends approximately 3 yr beyond PPTA DR2 [69], maintaining typical observing cadences of 3 weeks [19]. The timing precision varies across the pulsar sample, with the best-timed pulsars achieving root-mean-square residuals of ~ 100 ns.

The search for GW signals in PTA data requires a comprehensive description of stochastic processes affecting pulse arrival times. Following detailed noise analy-

ses of individual PPTA pulsars [70, 71], we model multiple noise components including both time-correlated (red) and uncorrelated (white) processes. The white noise model incorporates a scale parameter on the time-of-arrival uncertainties (EFAC), an added variance (EQUAD), and a per-epoch variance (ECORR) for each backend/receiver system [72]. Time-correlated noise is modeled using power-law processes for spin noise and dispersion measure variations. Additional components, such as, chromatic effects (scattering variations, band-specific noise), system-specific instrumental effects, and environmental contributions (solar wind variations, interstellar medium effects, magnetospheric events) are included [71]. These noise components are implemented using Bayesian inference with Gaussian processes through the **Enterprise** [73] software package.

The SGWB manifests as a common process across all pulsars, characterized by the cross-power spectral density [74]:

$$S_{IJ}(f) = \frac{H_0^2}{16\pi^4 f^5} \Gamma_{IJ}(\xi) \Omega_{\text{GW}}(f), \quad (22)$$

where $H_0 = 67.4 \text{ km s}^{-1} \text{ Mpc}^{-1}$ is the Hubble constant [75]. Here, Γ_{IJ} represents the Hellings-Downs correlation coefficients [22] between pulsars I and J given by

$$\Gamma_{IJ} = \frac{3}{2} \left(\frac{1 - \cos \xi}{2} \right) \ln \frac{1 - \cos \xi}{2} - \frac{1 - \cos \xi}{8} + \frac{1}{2}, \quad (23)$$

where ξ is the angular separation between pulsars I and J . We model the common process using 15 frequency components. In the nonminimal derivative coupling model, $\Omega_{\text{GW}}(f)$ is characterized by three parameters: coupling position ϕ_c , coupling peak height ω_L , and coupling smoothing scale σ . Based on theoretical constraints discussed in Sec. II B, we adopt uniform priors: $\phi_c/M_{\text{P}} \in [3, 4]$, $\log_{10} \omega_L \in [4, 8]$, and $\log_{10} \sigma \in [-10, -6]$.

For model selection, we compute Bayes factors defined as:

$$\mathcal{BF} \equiv \frac{\text{Pr}(\mathcal{D}|\mathcal{M}_2)}{\text{Pr}(\mathcal{D}|\mathcal{M}_1)}, \quad (24)$$

where $\text{Pr}(\mathcal{D}|\mathcal{M})$ represents the evidence for model \mathcal{M} given data \mathcal{D} . Following standard interpretation [76], $\mathcal{BF} \leq 3$ indicates the evidence for model \mathcal{M}_2 over \mathcal{M}_1 is “not worth more than a bare mention”. We implement all Bayesian analyses using **Enterprise**[73] and **Enterprise_extensions** [77] through the **PTArcade** [78, 79] wrapper, with Bayes factors estimated via the product-space method [80–83].

IV. RESULTS AND DISCUSSION

Using PPTA DR3, we constrain the parameters of our nonminimal derivative coupling inflation model. Fig. 4

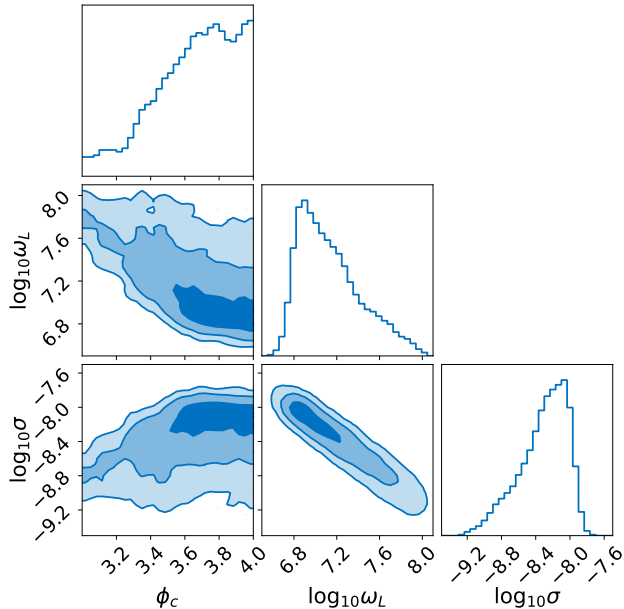


FIG. 4. Posterior distributions for the model parameters $\{\phi_c, \omega_L, \sigma\}$ constrained by PPTA DR3. The contours represent the 1σ , 2σ , and 3σ confidence levels in the two-dimensional plots.

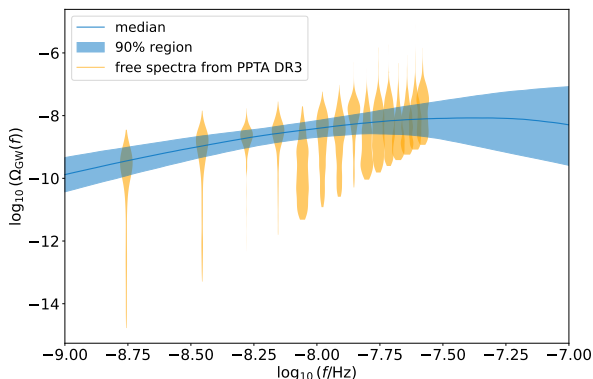


FIG. 5. Comparison between the predicted SIGW energy density spectrum from our inflationary model and PPTA DR3 observations. The solid blue line shows the median prediction from the posterior distribution, with the shaded region indicating the 90% credible interval. Orange violin plots represent the free spectra obtained from the PPTA DR3 [20].

shows the posterior distributions for the model parameters, yielding $\phi_c = 3.7_{-0.5}^{+0.3} M_{\text{P}}$, $\log \omega_L = 7.1_{-0.3}^{+0.6}$, and $\log \sigma = -8.3_{-0.6}^{+0.3}$ (quoted as median values with 90% credible intervals). These constraints demonstrate that PTA observations can effectively probe the shape of the coupling function $\theta(\phi)$, with ϕ_c determining its position, ω_L its peak height, and σ its smoothing scale.

To assess the model’s viability, we compare it with

the SMBHB hypothesis, where the GW energy density spectrum follows a power-law:

$$\Omega_{\text{PL}}(f) = \frac{2\pi^2 A_{\text{PL}}^2}{3H_0^2} \left(\frac{f}{f_{\text{yr}}}\right)^{5-\gamma_{\text{PL}}} f_{\text{yr}}^2, \quad (25)$$

with A_{PL} being the characteristic strain amplitude at $f_{\text{yr}} = 1/\text{yr}$ and $\gamma_{\text{PL}} = 13/3$ the expected spectral index. The Bayes factor between our model and the power-law model is 0.9, indicating that current sensitivity of PPTA data is insufficient to distinguish between these scenarios.

Fig. 5 presents the posterior predictive distribution for the SIGW energy density spectrum from our model. The median prediction (blue line) and 90% credible region (shaded area) are consistent with the free spectrum estimates from PPTA DR3 (orange violins), supporting the viability of our model.

Our analysis demonstrates a couple of key advances. First, we have developed an analytical approximation for the primordial curvature power spectrum in non-minimal derivative coupling inflation, avoiding computationally expensive numerical solutions of the Mukhanov-Sasaki equations. This approximation reduces computation time from minutes per parameter set to effectively instantaneous calculations while maintaining accuracy, enabling efficient exploration of the parameter space. Second, we have demonstrated that PTA observations can effectively constrain inflationary models with enhanced small-scale power spectra. This establishes PTAs as a powerful complement to CMB observations, extending our ability to probe inflationary dynamics across an unprecedented range of scales.

ACKNOWLEDGMENTS

This work has been carried out by the Parkes Pulsar Timing Array, which is part of the International Pulsar Timing Array. The Parkes radio telescope (“Murriyang”) is part of the Australia Telescope, which is funded by the Commonwealth Government for operation as a National Facility managed by CSIRO. This work was supported in part by the National Key Research and Development Program of China Grant No. 2020YFC2201502; the National Natural Science Foundation of China under Grants No. 12405056, No. 12305057, No. 12275080, No. 12203004, No. 12103069 and No. 12075084; the innovative research group of Hunan Province under Grant No. 2024JJ1006; and the Fundamental Research Funds for the Central Universities. VDM is supported via the Australian Research Council (ARC) Centre of Excellence CE170100004 and CE230100016 and receives support from the Australian Government Research Training Program.

Appendix A: Mukhanov-Sasaki equation

Starting from the action given in Eq. (1), we can derive the second-order action for the curvature perturbation \mathcal{R} [60, 64, 66, 84]:

$$S^{(2)} = \int dt d^3x a^2 Q_s \left[\dot{\mathcal{R}}^2 - \frac{c_s^2}{a^2} (\partial_i \mathcal{R})^2 \right], \quad (\text{A1})$$

where the kinetic coefficient Q_s is given by

$$Q_s = \frac{w_1(4w_1w_3 + 9w_2^2)}{3w_2^2}. \quad (\text{A2})$$

Here the coefficients w_i are defined as:

$$w_1 = M_P^2(1 - 2\delta_D), \quad (\text{A3})$$

$$w_2 = 2HM_P^2(1 - 6\delta_D), \quad (\text{A4})$$

$$w_3 = -3H^2M_P^2(3 - \delta_X + 36\delta_D), \quad (\text{A5})$$

$$w_4 = M_P^2(1 + 2\delta_D) \quad (\text{A6})$$

with

$$\delta_D = \frac{\kappa^4 \dot{\phi}^2 \theta}{4}, \quad \delta_X = \frac{\kappa^2 \dot{\phi}^2}{2H^2}. \quad (\text{A7})$$

From this second-order action, we can derive the Mukhanov-Sasaki equation:

$$u_k'' + \left(c_s^2 k^2 - \frac{z''}{z} \right) u_k = 0, \quad (\text{A8})$$

where we have introduced a variable $u_k \equiv z\mathcal{R}_k$ with $z \equiv a\sqrt{2Q_s}$. The power spectrum of curvature perturbations can then be expressed as:

$$\mathcal{P}_{\mathcal{R}}(k) = \frac{k^3}{2\pi^2} \left| \frac{u_k}{z} \right|^2. \quad (\text{A9})$$

Appendix B: Approximate Solution for $H/\dot{\phi}$

In this appendix, we derive the solution presented in Eq. (10) by analyzing different evolutionary stages of the system. The full dynamics are governed by Eqs. (3) and (4), which can be simplified based on the studies in [60] showing that $-\dot{H}/H^2 \ll 1$ and $\kappa^2 \dot{\phi}^2 / (2H^2) \ll 1$ hold throughout both the SR and USR stages. These conditions allow us to write

$$3H^2 \simeq \kappa^2 V, \quad (\text{B1})$$

$$(1 + 3\kappa^2 H^2 \theta) \ddot{\phi} + 3H(1 + 3\kappa^2 H^2 \theta) \dot{\phi} + \frac{3}{2} \kappa^2 H^2 \theta_{,\phi} \dot{\phi}^2 + V_{,\phi} \simeq 0. \quad (\text{B2})$$

In the following we analyze these equations in three distinct regimes.

1. Slow-Roll Regime

In the SR regime, we have $\ddot{\phi}/H\dot{\phi} \ll 1$, $-\dot{H}/H^2 \ll 1$, and $\theta_{,\phi} \ll \theta$. Although θ is small, it still contributes to the number of e-folds N . Under these conditions, Eq. (B2) reduces to

$$3H(1 + 3\kappa^2 H^2 \theta) \dot{\phi} + V_{,\phi} \simeq 0, \quad (\text{B3})$$

which yields the solution

$$\frac{H}{\dot{\phi}} = \frac{-3H^2(1 + 3\kappa^2 H^2 \theta)}{V_{,\phi}}. \quad (\text{B4})$$

2. Ultra-Slow-Roll Regime

In the USR regime, where $|\phi - \phi_c| < \sigma/\kappa$, the condition $\kappa^2 \dot{\phi}^2 / (2H^2) \ll 1$ implies

$$(1 + 9\kappa^2 H^2 \theta) \dot{\phi}^2 \simeq 0. \quad (\text{B5})$$

Taking the time derivative on the above equation and using $|\dot{H}/H^2| \ll 1$ lead to

$$\ddot{\phi} = -\frac{1}{2} \frac{9\kappa^2 H^2 \theta_{,\phi}}{1 + 9\kappa^2 H^2 \theta} \dot{\phi}^2. \quad (\text{B6})$$

Substituting this into Eq. (B2) and noting that $\kappa^2 H^2 \theta \gg 1$ in this regime, one can obtain

$$\frac{H}{\dot{\phi}} = -\frac{9\kappa^2 H^4 \theta}{V_{,\phi}}. \quad (\text{B7})$$

3. Transition Regime

Between the SR and USR stages ($1 \gg |\phi - \phi_c| \gg \sigma/\kappa$), there is a transition stage. Previous studies in [61] found a linear solution $\dot{\phi} \propto (\phi - \phi_c)$, implying

$$\ddot{\phi} = \frac{1}{\phi - \phi_c} \dot{\phi}^2, \quad (\text{B8})$$

which is approximately equivalent to

$$\ddot{\phi} = -\frac{3\kappa^2 H^2 \theta_{,\phi}}{1 + 3\kappa^2 H^2 \theta} \dot{\phi}^2. \quad (\text{B9})$$

Substituting this into Eq. (B2) and requiring consistency with the SR solution when $\theta = \theta_{,\phi} = 0$, we have

$$\frac{H}{\dot{\phi}} = -\frac{3H^2 \left(3(1 + 3\kappa^2 H^2 \theta) + \sqrt{6V_{,\phi} \theta_{,\phi} + 9(1 + 3\kappa^2 H^2 \theta)^2} \right)}{6V_{,\phi}}. \quad (\text{B10})$$

Combining Eqs. (B4), (B10), and (B7) with (B1) yields Eq. (10).

Appendix C: Derivation of the mapping between ϕ and k

This appendix provides a detailed derivation of the mapping relationship between ϕ and k from Eq. (10). We employ several approximations to make the integration tractable while maintaining physical consistency in different regions of the field space.

1. Basic Mapping for Minimal derivative Coupling

We first consider the minimal derivative coupling case where $\theta = 0$. In this limit, Eq. (10) reduces to

$$\frac{H}{\dot{\phi}} \simeq -\frac{\kappa^2 V}{V_{,\phi}}. \quad (\text{C1})$$

Combining Eqs. (5), (12), (3), and (11), we obtain

$$k(\phi) = \sqrt{\frac{\lambda}{3}} \phi^{\frac{p}{2}} e^{-\frac{\kappa^2 \phi^2}{2p}}. \quad (\text{C2})$$

Since the power-law term $\phi^{p/2}$ varies slowly compared to the exponential term, we can approximate it at a fixed value, e.g., at ϕ_c , yielding the inverse function:

$$\phi(k) = \sqrt{-\frac{2p}{\kappa^2} \ln \left(\frac{\sqrt{3}k}{\sqrt{\lambda \phi_c^{\frac{p}{2}}}} \right)}. \quad (\text{C3})$$

2. Extension to Non-minimal Coupling

For the non-minimal coupling case with θ given by Eq. (2), we need to consider different regions of the field space. We find that Eq. (10) can be expressed detailedly as:

$$\frac{H}{\dot{\phi}} \simeq \begin{cases} -\frac{\kappa^2 V(1+\kappa^4 V\theta)}{V_{,\phi}}, & \text{for } |\phi - \phi_c| > \kappa^2 \omega \lambda \sigma \phi_c^p \\ -\frac{\kappa^2 V(3(1+\kappa^4 V\theta)+3+\sqrt{6V_{,\phi}\theta_{,\phi}+9(\kappa^4 V\theta)^2})}{6V_{,\phi}}, & \text{for } \kappa^2 \omega \lambda \sigma \phi_c^p > |\phi - \phi_c| > \frac{\sigma}{\kappa} \\ -\frac{\kappa^6 V^2 \theta}{V_{,\phi}}, & \text{for } \frac{\sigma}{\kappa} > |\phi - \phi_c|. \end{cases} \quad (\text{C4})$$

The different regions of $|\phi - \phi_c|$ in Eq. (C4) are chosen based on physical considerations. The first region $|\phi - \phi_c| > \kappa^2 \omega \lambda \sigma \phi_c^p$ comes from the condition $\kappa^4 V\theta < 1$. In this regime, we have $-6V_{,\phi}\theta_{,\phi} \ll 9(1+\kappa^4 V\theta)^2$, allowing us to neglect the $\theta_{,\phi}$ term. When $\kappa^4 V\theta > 1$, we find θ grows rapidly, which means that $V_{,\phi}\theta_{,\phi} > 1$ and $\kappa^4 V\theta \gg 1$ are satisfied quickly. Then, we have $\sqrt{6V_{,\phi}\theta_{,\phi} + 9(1+\kappa^4 V\theta)^2} \simeq 3 + \sqrt{6V_{,\phi}\theta_{,\phi} + 9(\kappa^4 V\theta)^2}$. Further considering the properties of coupling function shown in C3, we divide the region of $\kappa^4 V\theta > 1$ into two parts.

Since V and $V_{,\phi}$ vary much more slowly than θ and $\theta_{,\phi}$, we can use $V^c = V(\phi_c)$ and $V_{,\phi}^c = V_{,\phi}(\phi_c)$ to replace V and $V_{,\phi}$ when they appear in terms including θ and $\theta_{,\phi}$. So, Eq. (C4) can be approximated as

$$\frac{H}{\dot{\phi}} \simeq \begin{cases} -\frac{\kappa^2 V}{V_{,\phi}} - \frac{\kappa^6 V^c \theta^2}{V_{,\phi}^c}, & \text{for } |\phi - \phi_c| > \kappa^2 \omega \lambda \sigma \phi_c^p \\ -\frac{\kappa^2 V}{V_{,\phi}} - \frac{\kappa^6 V^c \theta^2}{2V_{,\phi}^c} - \frac{\kappa^2 V^c (\sqrt{6V_{,\phi}^c \theta_{,\phi} + 9(\kappa^4 V^c \theta)^2})}{6V_{,\phi}^c}, & \text{for } \kappa^2 \omega \lambda \sigma \phi_c^p > |\phi - \phi_c| > \frac{\sigma}{\kappa} \\ -\frac{\kappa^6 V^c \theta^2}{V_{,\phi}^c}, & \text{for } \frac{\sigma}{\kappa} > |\phi - \phi_c|. \end{cases} \quad (\text{C5})$$

3. Approximation of the Coupling Function

The coupling function θ can be approximated as [61]

$$\theta \simeq \begin{cases} +\frac{\omega \sigma}{\kappa(\phi - \phi_c)}, & \text{for } \phi > \phi_c + \frac{\sigma}{\kappa} \\ \frac{\omega \sigma}{\sqrt{\kappa^2(\phi - \phi_c)^2 + \sigma^2}}, & \text{for } |\phi - \phi_c| \leq \frac{\sigma}{\kappa} \\ -\frac{\omega \sigma}{\kappa(\phi - \phi_c)}, & \text{for } \phi < \phi_c - \frac{\sigma}{\kappa} \end{cases} \quad (\text{C6})$$

and $\theta_{,\phi}$ can be expressed as

$$\theta_{,\phi} \simeq \begin{cases} -\frac{\omega \sigma}{\kappa^2(\phi - \phi_c)^2}, & \text{for } \phi > \phi_c \\ +\frac{\omega \sigma}{\kappa^2(\phi - \phi_c)^2}, & \text{for } \phi < \phi_c. \end{cases} \quad (\text{C7})$$

4. Derivation of the Final Mapping Relation

Using Eqs. (C6) and (C7), we find that Eq. (C5) can be further expressed as:

$$\frac{H}{\dot{\phi}} \simeq \begin{cases} -\frac{\kappa^2 V}{V_{,\phi}} - \frac{\kappa^6 V c^2}{V_{,\phi}^c} \frac{\omega \sigma}{\kappa(\phi - \phi_c)}, & \phi > \phi_c + \kappa^2 \omega \lambda \sigma \phi_c^p \\ -\frac{\kappa^2 V}{V_{,\phi}} + \mathcal{F}_1 \frac{\omega \sigma}{\kappa(\phi - \phi_c)}, & \phi_c + \frac{\sigma}{\kappa} < \phi < \phi_c + \kappa^2 \omega \lambda \sigma \phi_c^p \\ -\frac{\kappa^6 V c^2}{V_{,\phi}^c} \frac{\omega \sigma}{\sqrt{\kappa^2 (\phi - \phi_c)^2 + \sigma^2}}, & |\phi - \phi_c| < \frac{\sigma}{\kappa} \\ -\frac{\kappa^2 V}{V_{,\phi}} - \mathcal{F}_2 \frac{\omega \sigma}{\kappa(\phi - \phi_c)}, & \phi_c - \kappa^2 \omega \lambda \sigma \phi_c^p < \phi < \phi_c - \frac{\sigma}{\kappa} \\ -\frac{\kappa^2 V}{V_{,\phi}} + \frac{\kappa^6 V c^2}{V_{,\phi}^c} \frac{\omega \sigma}{\kappa(\phi - \phi_c)}, & \phi < \phi_c - \kappa^2 \omega \lambda \sigma \phi_c^p \end{cases} \quad (\text{C8})$$

where

$$\mathcal{F}_1 = -\frac{\kappa^6 V c^2}{2V_{,\phi}^c} - \frac{\kappa^2 V c}{6V_{,\phi}^c} \sqrt{-6V_{,\phi}^c \frac{\kappa^2}{\omega \sigma} + 9(\kappa^4 V c)^2}, \quad (\text{C9})$$

$$\mathcal{F}_2 = -\frac{\kappa^6 V c^2}{2V_{,\phi}^c} - \frac{\kappa^2 V c}{6V_{,\phi}^c} \sqrt{6V_{,\phi}^c \frac{\kappa^2}{\omega \sigma} + 9(\kappa^4 V c)^2}. \quad (\text{C10})$$

While these approximations are not exact, they are sufficient for our calculations. Integrating this piecewise function according to Eq. (11) yields $N(\phi)$ and consequently $k(\phi)$. After appropriate approximations, we can obtain the inverse function $\phi(k)$ (setting $\kappa^{-1} = M_P = 1$ for simplicity):

$$\phi(k) = \begin{cases} \phi_1(k), & 0 < k < k_1 \\ \phi_2(k), & k_1 < k < k_2 \\ \phi_3(k), & k_2 < k < k_3 \\ \phi_4(k), & k_3 < k < k_4 \\ \phi_5(k), & k_4 < k \end{cases} \quad (\text{C11})$$

where the transition wavenumbers are given by:

$$k_1 = \left(\frac{\lambda(\phi_c + \omega \lambda \sigma \phi_c^p)^p}{3} \right)^{\frac{1}{2}} e^{N_1 + N_2 + N_3 + N_4}, \quad (\text{C12})$$

$$k_2 = \left(\frac{\lambda(\phi_c + \sigma)^p}{3} \right)^{\frac{1}{2}} e^{N_1 + N_2 + N_3}, \quad (\text{C13})$$

$$k_3 = \left(\frac{\lambda(\phi_c - \sigma)^p}{3} \right)^{\frac{1}{2}} e^{N_1 + N_2}, \quad (\text{C14})$$

$$k_4 = \left(\frac{\lambda(\phi_c - \omega \lambda \sigma \phi_c^p)^p}{3} \right)^{\frac{1}{2}} e^{N_1}. \quad (\text{C15})$$

Here the auxiliary functions N_i are defined as:

$$N_1 = \frac{2\lambda\sigma\phi_c^{1+p}\omega \ln[\lambda\sigma\phi_c^{-1+p}\omega] - (\phi_c - \lambda\sigma\phi_c^p\omega)^2}{2p}, \quad (\text{C16})$$

$$N_2 = \frac{(\phi_c - \lambda\sigma\phi_c^p\omega)^2 - (\phi_c - \sigma)^2}{2p} + \mathcal{G}_1 \ln \left[\frac{1}{\lambda\omega\phi_c^p} \right], \quad (\text{C17})$$

$$N_3 = \frac{\lambda\omega\sigma\phi_c^{1+p}}{2p} \ln \left[\frac{(\sqrt{2\sigma} - \sigma)^2}{(\sqrt{2\sigma} + \sigma)^2} \right], \quad (\text{C18})$$

$$N_4 = \frac{(\phi_c + \sigma)^2 - (\phi_c + \lambda\omega\sigma\phi_c^p)^2}{2p} + \mathcal{G}_2 \ln \left[\frac{1}{\lambda\omega\phi_c^p} \right], \quad (\text{C19})$$

with

$$\mathcal{G}_1 = \frac{\lambda\omega\sigma\phi_c}{6p} \left(3\phi_c^p + \sqrt{3\phi_c^p[3\phi_c^p + 2p(\sigma\lambda\omega\phi_c)^{-1}]} \right), \quad (\text{C20})$$

$$\mathcal{G}_2 = \frac{\lambda\omega\sigma\phi_c}{6p} \left(3\phi_c^p + \sqrt{3\phi_c^p[3\phi_c^p - 2p(\sigma\lambda\omega\phi_c)^{-1}]} \right). \quad (\text{C21})$$

The corresponding field values in each region are given by:

$$\phi_1(k) = \left\{ 2p(N_1 + N_2 + N_3 + N_4) + 2(\phi_c + \lambda\omega\sigma\phi_c^p)^2 - (\phi_c + \sigma)^2 - 2p \ln \left[\frac{\sqrt{3}k}{\sqrt{\lambda\phi_c^p}} \right] \right\}^{\frac{1}{2}}, \quad (\text{C22})$$

$$\phi_2(k) = \phi_c + \sigma \left(\frac{\sqrt{3}e^{-N_1-N_2-N_3}k}{\sqrt{\lambda\phi_c^p}} \right)^{-3+\alpha}, \quad (\text{C23})$$

$$\phi_3(k) = (\phi_c + \sigma) \left[\left(\frac{\lambda(\phi_c + \sigma)}{3} \right)^{\frac{1}{2}} e^{N_1+N_2+N_3} \right]^{-\beta} k^\beta, \quad (\text{C24})$$

$$\phi_4(k) = \phi_c - \sigma\lambda\omega\phi_c^p \left(\frac{\sqrt{3}e^{-N_1+\gamma}k}{\sqrt{\lambda\phi_c^p}} \right)^{-3+\delta}, \quad (\text{C25})$$

$$\phi_5(k) = \left\{ 2p(N_1 + N_2) + (\phi_c - \omega\lambda\sigma\phi_c^p)^2 - 2p \ln \left[\frac{\sqrt{3}k}{\sqrt{\lambda\phi_c^p}} \right] + \epsilon \right\}^{\frac{1}{2}}, \quad (\text{C26})$$

where

$$\alpha = \sqrt{3}\lambda^{-1}\phi_c^{-p} \sqrt{\lambda\phi_c^p(3\lambda\phi_c^p - 2p(\sigma\omega\phi_c)^{-1})}, \quad (\text{C27})$$

$$\beta = N_3^{-1} \ln \left(\frac{\phi_c + \sigma}{\phi_c - \sigma} \right), \quad (\text{C28})$$

$$\gamma = \frac{(\phi_c - \sigma)^2 - (\phi_c - \sigma\lambda\omega\phi_c^p)^2}{2p}, \quad (\text{C29})$$

$$\delta = \sqrt{3}\lambda^{-1}\phi_c^{-p} \sqrt{\lambda\phi_c^p(3\lambda\phi_c^p + 2p(\sigma\omega\phi_c)^{-1})}, \quad (\text{C30})$$

$$\epsilon = -\frac{\phi_c}{3} \left(3\omega\lambda\sigma\phi_c^p + \sqrt{3\omega\lambda\sigma\phi_c^{-1+p}(2p + 3\omega\lambda\sigma\phi_c^{1+p})} \right) \ln \left[\frac{1}{\omega\lambda\phi_c^p} \right]. \quad (\text{C31})$$

-
- [1] Alan H. Guth, “The Inflationary Universe: A Possible Solution to the Horizon and Flatness Problems,” *Phys. Rev. D* **23**, 347–356 (1981).
- [2] Andrei D. Linde, “A New Inflationary Universe Scenario: A Possible Solution of the Horizon, Flatness, Homogeneity, Isotropy and Primordial Monopole Problems,” *Phys. Lett. B* **108**, 389–393 (1982).
- [3] Andreas Albrecht and Paul J. Steinhardt, “Cosmology for Grand Unified Theories with Radiatively Induced Symmetry Breaking,” *Phys. Rev. Lett.* **48**, 1220–1223 (1982).
- [4] Alan H. Guth and S. Y. Pi, “Fluctuations in the New Inflationary Universe,” *Phys. Rev. Lett.* **49**, 1110–1113 (1982).
- [5] David H. Lyth and Antonio Riotto, “Particle physics models of inflation and the cosmological density perturbation,” *Phys. Rept.* **314**, 1–146 (1999), arXiv:hep-ph/9807278.
- [6] Y. Akrami *et al.* (Planck), “Planck 2018 results. X. Constraints on inflation,” *Astron. Astrophys.* **641**, A10 (2020), arXiv:1807.06211 [astro-ph.CO].
- [7] Stephen Hawking, “Gravitationally collapsed objects of very low mass,” *Mon. Not. Roy. Astron. Soc.* **152**, 75 (1971).
- [8] Bernard J. Carr and S. W. Hawking, “Black holes in the early Universe,” *Mon. Not. Roy. Astron. Soc.* **168**, 399–415 (1974).
- [9] Misao Sasaki, Teruaki Suyama, Takahiro Tanaka,

- and Shuichiro Yokoyama, “Primordial black holes—perspectives in gravitational wave astronomy,” *Class. Quant. Grav.* **35**, 063001 (2018), arXiv:1801.05235 [astro-ph.CO].
- [10] Simeon Bird, Ilias Cholis, Julian B. Muñoz, Yacine Ali-Haïmoud, Marc Kamionkowski, Ely D. Kovetz, Alvise Raccanelli, and Adam G. Riess, “Did LIGO detect dark matter?” *Phys. Rev. Lett.* **116**, 201301 (2016), arXiv:1603.00464 [astro-ph.CO].
- [11] Misao Sasaki, Teruaki Suyama, Takahiro Tanaka, and Shuichiro Yokoyama, “Primordial Black Hole Scenario for the Gravitational-Wave Event GW150914,” *Phys. Rev. Lett.* **117**, 061101 (2016), [Erratum: Phys.Rev.Lett. 121, 059901 (2018)], arXiv:1603.08338 [astro-ph.CO].
- [12] Zu-Cheng Chen and Alex Hall, “Confronting primordial black holes with LIGO-Virgo-KAGRA and the Einstein Telescope,” (2024), arXiv:2402.03934 [astro-ph.CO].
- [13] Naoki Seto and Asantha Cooray, “Search for small-mass black hole dark matter with space-based gravitational wave detectors,” *Phys. Rev. D* **70**, 063512 (2004), arXiv:astro-ph/0405216.
- [14] Ryo Saito and Jun’ichi Yokoyama, “Gravitational wave background as a probe of the primordial black hole abundance,” *Phys. Rev. Lett.* **102**, 161101 (2009), [Erratum: Phys.Rev.Lett. 107, 069901 (2011)], arXiv:0812.4339 [astro-ph].
- [15] J. Antoniadis *et al.* (EPTA), “The second data release from the European Pulsar Timing Array - I. The dataset and timing analysis,” *Astron. Astrophys.* **678**, A48 (2023), arXiv:2306.16224 [astro-ph.HE].
- [16] J. Antoniadis *et al.* (EPTA, InPTA:), “The second data release from the European Pulsar Timing Array - III. Search for gravitational wave signals,” *Astron. Astrophys.* **678**, A50 (2023), arXiv:2306.16214 [astro-ph.HE].
- [17] Gabriella Agazie *et al.* (NANOGrav), “The NANOGrav 15 yr Data Set: Observations and Timing of 68 Millisecond Pulsars,” *Astrophys. J. Lett.* **951**, L9 (2023), arXiv:2306.16217 [astro-ph.HE].
- [18] Gabriella Agazie *et al.* (NANOGrav), “The NANOGrav 15 yr Data Set: Evidence for a Gravitational-wave Background,” *Astrophys. J. Lett.* **951**, L8 (2023), arXiv:2306.16213 [astro-ph.HE].
- [19] Andrew Zic *et al.*, “The Parkes Pulsar Timing Array third data release,” *Publ. Astron. Soc. Austral.* **40**, e049 (2023), arXiv:2306.16230 [astro-ph.HE].
- [20] Daniel J. Reardon *et al.*, “Search for an Isotropic Gravitational-wave Background with the Parkes Pulsar Timing Array,” *Astrophys. J. Lett.* **951**, L6 (2023), arXiv:2306.16215 [astro-ph.HE].
- [21] Heng Xu *et al.*, “Searching for the Nano-Hertz Stochastic Gravitational Wave Background with the Chinese Pulsar Timing Array Data Release I,” *Res. Astron. Astrophys.* **23**, 075024 (2023), arXiv:2306.16216 [astro-ph.HE].
- [22] R. w. Hellings and G. s. Downs, “UPPER LIMITS ON THE ISOTROPIC GRAVITATIONAL RADIATION BACKGROUND FROM PULSAR TIMING ANALYSIS,” *Astrophys. J. Lett.* **265**, L39-L42 (1983).
- [23] Matthew T. Miles *et al.*, “The MeerKAT Pulsar Timing Array: The 4.5-year data release and the noise and stochastic signals of the millisecond pulsar population,” (2024), 10.1093/mnras/stae2572, arXiv:2412.01148 [astro-ph.HE].
- [24] Matthew T. Miles *et al.*, “The MeerKAT Pulsar Timing Array: The first search for gravitational waves with the MeerKAT radio telescope,” (2024), 10.1093/mnras/stae2571, arXiv:2412.01153 [astro-ph.HE].
- [25] Gabriella Agazie *et al.* (NANOGrav), “The NANOGrav 15 yr Data Set: Constraints on Supermassive Black Hole Binaries from the Gravitational-wave Background,” *Astrophys. J. Lett.* **952**, L37 (2023), arXiv:2306.16220 [astro-ph.HE].
- [26] John Ellis, Malcolm Fairbairn, Gert Hütsi, Juhan Raidal, Juan Urrutia, Ville Vaskonen, and Hardi Veermäe, “Gravitational waves from supermassive black hole binaries in light of the NANOGrav 15-year data,” *Phys. Rev. D* **109**, L021302 (2024), arXiv:2306.17021 [astro-ph.CO].
- [27] Yan-Chen Bi, Yu-Mei Wu, Zu-Cheng Chen, and Qing-Guo Huang, “Implications for the supermassive black hole binaries from the NANOGrav 15-year data set,” *Sci. China Phys. Mech. Astron.* **66**, 120402 (2023), arXiv:2307.00722 [astro-ph.CO].
- [28] Adeela Afzal *et al.* (NANOGrav), “The NANOGrav 15 yr Data Set: Search for Signals from New Physics,” *Astrophys. J. Lett.* **951**, L11 (2023), [Erratum: Astrophys.J.Lett. 971, L27 (2024), Erratum: Astrophys.J. 971, L27 (2024)], arXiv:2306.16219 [astro-ph.HE].
- [29] J. Antoniadis *et al.* (EPTA, InPTA), “The second data release from the European Pulsar Timing Array - IV. Implications for massive black holes, dark matter, and the early Universe,” *Astron. Astrophys.* **685**, A94 (2024), arXiv:2306.16227 [astro-ph.CO].
- [30] Yu-Mei Wu, Zu-Cheng Chen, and Qing-Guo Huang, “Cosmological interpretation for the stochastic signal in pulsar timing arrays,” *Sci. China Phys. Mech. Astron.* **67**, 240412 (2024), arXiv:2307.03141 [astro-ph.CO].
- [31] John Ellis, Malcolm Fairbairn, Gabriele Franciolini, Gert Hütsi, Antonio Iovino, Marek Lewicki, Martti Raidal, Juan Urrutia, Ville Vaskonen, and Hardi Veermäe, “What is the source of the PTA GW signal?” *Phys. Rev. D* **109**, 023522 (2024), arXiv:2308.08546 [astro-ph.CO].
- [32] Daniel G. Figueroa, Mauro Pieroni, Angelo Ricciardone, and Peera Simakachorn, “Cosmological Background Interpretation of Pulsar Timing Array Data,” *Phys. Rev. Lett.* **132**, 171002 (2024), arXiv:2307.02399 [astro-ph.CO].
- [33] Kishore N. Ananda, Chris Clarkson, and David Wands, “The Cosmological gravitational wave background from primordial density perturbations,” *Phys. Rev. D* **75**, 123518 (2007), arXiv:gr-qc/0612013.
- [34] Daniel Baumann, Paul J. Steinhardt, Keitaro Takahashi, and Kiyotomo Ichiki, “Gravitational Wave Spectrum Induced by Primordial Scalar Perturbations,” *Phys. Rev. D* **76**, 084019 (2007), arXiv:hep-th/0703290.
- [35] Kazunori Kohri and Takahiro Terada, “Semianalytic calculation of gravitational wave spectrum nonlinearly induced from primordial curvature perturbations,” *Phys. Rev. D* **97**, 123532 (2018), arXiv:1804.08577 [gr-qc].
- [36] Zu-Cheng Chen, Chen Yuan, and Qing-Guo Huang, “Pulsar Timing Array Constraints on Primordial Black Holes with NANOGrav 11-Year Dataset,” *Phys. Rev. Lett.* **124**, 251101 (2020), arXiv:1910.12239 [astro-ph.CO].
- [37] Gabriele Franciolini, Antonio Iovino, Junior., Ville Vaskonen, and Hardi Veermäe, “Recent Gravitational Wave Observation by Pulsar Timing Arrays and Primordial Black Holes: The Importance of Non-Gaussianities,” *Phys. Rev. Lett.* **131**, 201401 (2023), arXiv:2306.17149 [astro-ph.CO].

- [38] Lang Liu, Zu-Cheng Chen, and Qing-Guo Huang, “Implications for the non-Gaussianity of curvature perturbation from pulsar timing arrays,” *Phys. Rev. D* **109**, L061301 (2024), arXiv:2307.01102 [astro-ph.CO].
- [39] Sai Wang, Zhi-Chao Zhao, Jun-Peng Li, and Qing-Hua Zhu, “Implications of pulsar timing array data for scalar-induced gravitational waves and primordial black holes: Primordial non-Gaussianity fNL considered,” *Phys. Rev. Res.* **6**, L012060 (2024), arXiv:2307.00572 [astro-ph.CO].
- [40] Zhu Yi, Qing Gao, Yungui Gong, Yue Wang, and Fengge Zhang, “Scalar induced gravitational waves in light of Pulsar Timing Array data,” *Sci. China Phys. Mech. Astron.* **66**, 120404 (2023), arXiv:2307.02467 [gr-qc].
- [41] Lang Liu, Zu-Cheng Chen, and Qing-Guo Huang, “Probing the equation of state of the early Universe with pulsar timing arrays,” *JCAP* **11**, 071 (2023), arXiv:2307.14911 [astro-ph.CO].
- [42] Shyam Balaji, Guillem Domènech, and Gabriele Franciolini, “Scalar-induced gravitational wave interpretation of PTA data: the role of scalar fluctuation propagation speed,” *JCAP* **10**, 041 (2023), arXiv:2307.08552 [gr-qc].
- [43] Lang Liu, You Wu, and Zu-Cheng Chen, “Simultaneously probing the sound speed and equation of state of the early Universe with pulsar timing arrays,” *JCAP* **04**, 011 (2024), arXiv:2310.16500 [astro-ph.CO].
- [44] Sai Wang, Zhi-Chao Zhao, and Qing-Hua Zhu, “Constraints on scalar-induced gravitational waves up to third order from a joint analysis of BBN, CMB, and PTA data,” *Phys. Rev. Res.* **6**, 013207 (2024), arXiv:2307.03095 [astro-ph.CO].
- [45] Qing-Hua Zhu, Zhi-Chao Zhao, Sai Wang, and Xin Zhang, “Unraveling the early universe’s equation of state and primordial black hole production with PTA, BBN, and CMB observations*,” *Chin. Phys. C* **48**, 125105 (2024), arXiv:2307.13574 [astro-ph.CO].
- [46] Zhi-Qiang You, Zhu Yi, and You Wu, “Constraints on primordial curvature power spectrum with pulsar timing arrays,” *JCAP* **11**, 065 (2023), arXiv:2307.04419 [gr-qc].
- [47] Zhu Yi, Zhi-Qiang You, and You Wu, “Model-independent reconstruction of the primordial curvature power spectrum from PTA data,” *JCAP* **01**, 066 (2024), arXiv:2308.05632 [astro-ph.CO].
- [48] Zhu Yi, Zhi-Qiang You, You Wu, Zu-Cheng Chen, and Lang Liu, “Exploring the NANOGrav signal and planet-mass primordial black holes through Higgs inflation,” *JCAP* **06**, 043 (2024), arXiv:2308.14688 [astro-ph.CO].
- [49] Keisuke Harigaya, Keisuke Inomata, and Takahiro Terada, “Induced gravitational waves with kination era for recent pulsar timing array signals,” *Phys. Rev. D* **108**, 123538 (2023), arXiv:2309.00228 [astro-ph.CO].
- [50] Zu-Cheng Chen, Jun Li, Lang Liu, and Zhu Yi, “Probing the speed of scalar-induced gravitational waves with pulsar timing arrays,” *Phys. Rev. D* **109**, L101302 (2024), arXiv:2401.09818 [gr-qc].
- [51] Zu-Cheng Chen and Lang Liu, “Can we distinguish the adiabatic fluctuations and isocurvature fluctuations with pulsar timing arrays?” (2024), arXiv:2402.16781 [astro-ph.CO].
- [52] William H. Kinney, “A Hamilton-Jacobi approach to nonslow roll inflation,” *Phys. Rev. D* **56**, 2002–2009 (1997), arXiv:hep-ph/9702427.
- [53] Shogo Inoue and Jun’ichi Yokoyama, “Curvature perturbation at the local extremum of the inflaton’s potential,” *Phys. Lett. B* **524**, 15–20 (2002), arXiv:hep-ph/0104083.
- [54] William H. Kinney, “Horizon crossing and inflation with large eta,” *Phys. Rev. D* **72**, 023515 (2005), arXiv:gr-qc/0503017.
- [55] Alexander Y. Kamenshchik, Alessandro Tronconi, Tereza Vardanyan, and Giovanni Venturi, “Non-Canonical Inflation and Primordial Black Holes Production,” *Phys. Lett. B* **791**, 201–205 (2019), arXiv:1812.02547 [gr-qc].
- [56] Guillermo Ballesteros, Jose Beltran Jimenez, and Mauro Pieroni, “Black hole formation from a general quadratic action for inflationary primordial fluctuations,” *JCAP* **06**, 016 (2019), arXiv:1811.03065 [astro-ph.CO].
- [57] Yi-Fu Cai, Xi Tong, Dong-Gang Wang, and Sheng-Feng Yan, “Primordial Black Holes from Sound Speed Resonance during Inflation,” *Phys. Rev. Lett.* **121**, 081306 (2018), arXiv:1805.03639 [astro-ph.CO].
- [58] Chao Chen and Yi-Fu Cai, “Primordial black holes from sound speed resonance in the inflaton-curvature mixed scenario,” *JCAP* **10**, 068 (2019), arXiv:1908.03942 [astro-ph.CO].
- [59] Zihan Zhou, Jie Jiang, Yi-Fu Cai, Misao Sasaki, and Shi Pi, “Primordial black holes and gravitational waves from resonant amplification during inflation,” *Phys. Rev. D* **102**, 103527 (2020), arXiv:2010.03537 [astro-ph.CO].
- [60] Chengjie Fu, Puxun Wu, and Hongwei Yu, “Primordial Black Holes from Inflation with Nonminimal Derivative Coupling,” *Phys. Rev. D* **100**, 063532 (2019), arXiv:1907.05042 [astro-ph.CO].
- [61] Chengjie Fu, Puxun Wu, and Hongwei Yu, “Scalar induced gravitational waves in inflation with gravitationally enhanced friction,” *Phys. Rev. D* **101**, 023529 (2020), arXiv:1912.05927 [astro-ph.CO].
- [62] Cristiano Germani and Alex Kehagias, “New Model of Inflation with Non-minimal Derivative Coupling of Standard Model Higgs Boson to Gravity,” *Phys. Rev. Lett.* **105**, 011302 (2010), arXiv:1003.2635 [hep-ph].
- [63] Cristiano Germani and Yuki Watanabe, “UV-protected (Natural) Inflation: Primordial Fluctuations and non-Gaussian Features,” *JCAP* **07**, 031 (2011), [Addendum: *JCAP* **07**, A01 (2011)], arXiv:1106.0502 [astro-ph.CO].
- [64] Shinji Tsujikawa, “Observational tests of inflation with a field derivative coupling to gravity,” *Phys. Rev. D* **85**, 083518 (2012), arXiv:1201.5926 [astro-ph.CO].
- [65] Eva Silverstein and Alexander Westphal, “Monodromy in the CMB: Gravity Waves and String Inflation,” *Phys. Rev. D* **78**, 106003 (2008), arXiv:0803.3085 [hep-th].
- [66] V. Mukhanov, *Physical Foundations of Cosmology* (Cambridge University Press, Oxford, 2005).
- [67] Keisuke Inomata and Tomohiro Nakama, “Gravitational waves induced by scalar perturbations as probes of the small-scale primordial spectrum,” *Phys. Rev. D* **99**, 043511 (2019), arXiv:1812.00674 [astro-ph.CO].
- [68] Jing Liu, Zong-Kuan Guo, and Rong-Gen Cai, “Analytical approximation of the scalar spectrum in the ultraslow-roll inflationary models,” *Phys. Rev. D* **101**, 083535 (2020), arXiv:2003.02075 [astro-ph.CO].
- [69] Matthew Kerr *et al.*, “The Parkes Pulsar Timing Array project: second data release,” *Publ. Astron. Soc. Austral.* **37**, e020 (2020), arXiv:2003.09780 [astro-ph.IM].
- [70] Boris Goncharov *et al.*, “Identifying and mitigating noise sources in precision pulsar timing data sets,” *Mon. Not. Roy. Astron. Soc.* **502**, 478–493 (2021), arXiv:2010.06109 [astro-ph.HE].
- [71] Daniel J. Reardon *et al.*, “The Gravitational-wave Background Null Hypothesis: Characterizing Noise in Mil-

- lisecond Pulsar Arrival Times with the Parkes Pulsar Timing Array,” *Astrophys. J. Lett.* **951**, L7 (2023), [arXiv:2306.16229 \[astro-ph.HE\]](#).
- [72] Z. Arzoumanian *et al.* (NANOGrav), “The NANOGrav Nine-year Data Set: Limits on the Isotropic Stochastic Gravitational Wave Background,” *Astrophys. J.* **821**, 13 (2016), [arXiv:1508.03024 \[astro-ph.GA\]](#).
- [73] Justin A. Ellis, Michele Vallisneri, Stephen R. Taylor, and Paul T. Baker, “Enterprise: Enhanced numerical toolbox enabling a robust pulsar inference suite,” Zenodo (2020).
- [74] Eric Thrane and Joseph D. Romano, “Sensitivity curves for searches for gravitational-wave backgrounds,” *Phys. Rev. D* **88**, 124032 (2013), [arXiv:1310.5300 \[astro-ph.IM\]](#).
- [75] N. Aghanim *et al.* (Planck), “Planck 2018 results. VI. Cosmological parameters,” *Astron. Astrophys.* **641**, A6 (2020), [Erratum: *Astron. Astrophys.* 652, C4 (2021)], [arXiv:1807.06209 \[astro-ph.CO\]](#).
- [76] Robert E. Kass and Adrian E. Raftery, “Bayes factors,” *Journal of the American Statistical Association* **90**, 773–795 (1995).
- [77] Stephen R. Taylor, Paul T. Baker, Jeffrey S. Hazboun, Joseph Simon, and Sarah J. Vigeland, “enterprise_extensions,” (2021), v2.4.3.
- [78] Andrea Mitridate, David Wright, Richard von Eckardstein, Tobias Schröder, Jonathan Nay, Ken Olum, Kai Schmitz, and Tanner Trickle, “PTArcade,” (2023), [arXiv:2306.16377 \[hep-ph\]](#).
- [79] Andrea Mitridate, “Ptarcade,” (2023), [10.5281/zenodo.7876430](#).
- [80] Bradley P. Carlin and Siddhartha Chib, “Bayesian model choice via markov chain monte carlo methods,” *Journal of the Royal Statistical Society. Series B (Methodological)* **57**, 473–484 (1995).
- [81] Simon J. Godsill, “On the relationship between markov chain monte carlo methods for model uncertainty,” *Journal of Computational and Graphical Statistics* **10**, 230–248 (2001).
- [82] Sonke Hee, Will Handley, Mike P. Hobson, and Anthony N. Lasenby, “Bayesian model selection without evidences: application to the dark energy equation-of-state,” *Mon. Not. Roy. Astron. Soc.* **455**, 2461–2473 (2016), [arXiv:1506.09024 \[astro-ph.CO\]](#).
- [83] Stephen R. Taylor, Rutger van Haasteren, and Alberto Sesana, “From Bright Binaries To Bumpy Backgrounds: Mapping Realistic Gravitational Wave Skies With Pulsar-Timing Arrays,” *Phys. Rev. D* **102**, 084039 (2020), [arXiv:2006.04810 \[astro-ph.IM\]](#).
- [84] Tsutomu Kobayashi, Masahide Yamaguchi, and Jun’ichi Yokoyama, “Generalized G-inflation: Inflation with the most general second-order field equations,” *Prog. Theor. Phys.* **126**, 511–529 (2011), [arXiv:1105.5723 \[hep-th\]](#).